Conductivity studies of dense yttrium-doped BaZrO$_3$ sintered at 1325 °C

Shanwen Tao, John T.S. Irvine*

School of Chemistry, University of Saint Andrews, Saint Andrews, Fife KY16 9ST, UK

Abstract

High-temperature proton conductors have wide applications in the areas of fuel cells, electrolysis and hydrogen separation. Barium zirconate-based materials are of interest due to their good stability and high protonic conductivity. The reported conductivity of these ceramic materials is generally less than 10^{-2} S/cm, even at high temperatures. This is not high enough for an electrolyte-supported device to achieve an ASR of less than $0.2 \Omega \, cm^2$ therefore thin film electrolytes are required for successful application. As BaZrO$_3$-based materials have to be sintered at temperatures as high as 1700 °C, this makes it difficult to find a suitable supporting electrode which will not undergo significant chemical reaction with the BaZrO$_3$-based electrolyte during fabrication of the required electrode supported electrolyte. In this paper, proton-conducting BaZr$_{0.8}$Y$_{0.2}$O$_{2.9}$ was successfully sintered at 1325 °C with a relative density of 96% via addition of 1 wt% ZnO. Fabrication of electrochemical cells using proton-conducting BaZr$_{0.8}$Y$_{0.2}$O$_{2.9}$ as the electrolyte thus becomes possible. The formula of the 1 wt% ZnO added sample is Ba$_{0.97}$Zr$_{0.77}$Y$_{0.19}$Zn$_{0.04}$O$_{3-\delta}$ which exhibits a tetragonal structure with space group $P4/mbm$ (127); $a = 5.9787(1)$ Å, $c = 4.2345(1)$ Å, $V = 151.36(1)$ Å^3. It was found that a solid solution was formed for a limited range of Zn doping. Conductivity has been studied as a function of atmosphere (air, dry and wet 5% H$_2$/Ar) with the changes in bulk and grain boundary on changing atmosphere being monitored as a function of time. The total conductivity of Ba$_{0.97}$Zr$_{0.77}$Y$_{0.19}$Zn$_{0.04}$O$_{3-\delta}$ is 1.0×10^{-3} S/cm above 600 °C therefore it may be used as a proton-conducting thin film electrolyte for efficient electrochemical devices at such temperatures. The grain boundary resistance is insignificant at high temperature for the well-sintered sample.
© 2007 Published by Elsevier Inc.

Keywords: Proton conductor; Conductivity; Sintering; BaZr$_{0.8}$Y$_{0.2}$O$_{2.9}$

1. Introduction

High-temperature proton-conducting materials have wide application in solid oxide fuel cells, electrolysis of steam and hydrogen separation, etc. [1–7]. In general, perovskite oxides AB$'_{1-x}$B$''_x$O$_{3-\delta}$ with A = Ca, Sr, Ba; B$'$ = Ce, Zr; B$''$ = Sc, Ln, etc. exhibit proton conduction over a certain temperature range and steam concentration. Among the oxides, Ln-doped BaCeO$_3$ exhibits the highest proton conductivity; however, these materials are unstable at high temperature in the presence of CO$_2$ and steam which are unavoidable in an electrochemical cell, particularly under solid oxide fuel cell conditions [8,9]. The stability of doped BaCeO$_3$ was improved by the introduction of Zr at the B-site [10,11] but the required sintering temperature of Zr-substituted BaCeO$_3$ is still above

1550 °C. Such a high sintering temperature makes it difficult to fabricate an effective electrochemical cell using these oxides as the electrolyte since it is difficult to find good electrode materials which can sustain so high a temperature without significant chemical reactions. It is also essentially impossible to retain the porous microstructure of electrodes and so the surface activity of the electrodes would be ruined after experiencing such a high-temperature sintering. This would make the electrode ineffective, notwithstanding the requirements and cost for the sintering facilities. Therefore, a major obstacle for application of BaZrO$_3$-based proton conductors is the high sintering temperature that is required.

The high grain boundary resistance of sintered BaZr$_{1-x}$Y$_x$O$_{3-\delta}$ (x = 0.1, 0.2) also limits the application of these materials although it may be improved by the introduction of cerium at the B-site [7]. It has also been reported that, in the BaCe$_{1-x}$Y$_x$O$_{3-\delta}$ ($x \leqslant 0.3$) series, the conductivity increases with increasing yttrium content [12].

*Corresponding author. Fax: +44 1334 463 808.
E-mail address: jtsi@st-andrews.ac.uk (J.T.S. Irvine).

It is also reported that the conductivity of its analogue $BaZr_{1-x}Y_xO_{3-\delta}$ increases with increasing yttrium content as well [13]. The conductivity of $BaZr_{1-x}Y_xO_{3-\delta}$ with $x = 0.1$ and 0.2 has been investigated by several research groups [14–17] although significant differences in conductivities have been reported. This may be attributed to the synthetic history of the materials and the measuring condition owing to their sensitivity to steam concentration and the slow kinetic process of water absorption, which was suggested by Snijkers et al. [18]. Dense $BaZrO_3$ ceramic was achieved by sintering at very high temperature, e.g. 1700 °C [15,19]. The chemical compatibility of candidate oxide cathodes for $BaZrO_3$ electrolytes has also been investigated [20].

In our laboratory, it was found that ZnO doping can effectively enhance the sintering of $BaZrO_3$-based materials [21,22]. A similar effect was also reported independently by Haile et al. [23], principally attributing this enhancement in sintering to ZnO acting as a sintering aid. In this previous study, the conductivity of $BaZr_{0.85}Y_{0.15}O_{3-\delta}$ has been investigated in different nitrogen atmospheres and an open circuit voltage (OCV) of 1 V obtained in a H_2/air EMF cell [23]. Previously we have briefly reported on enhanced sintering of barium zirconates and barium cerate/zirconates [22], here we present detailed studies on the solid state chemistry, ceramic processing and conductivity in different atmospheres of zinc-oxide added $BaZr_{0.8}Y_{0.2}O_{3-\delta}$ and the related solid solution $Ba_{0.97}Zr_{0.8}Y_{0.2-x}Zn_xO_{3-\delta}$.

2. Experimental

The nominal $BaZr_{0.8}Y_{0.2}O_{3-\delta}$ powder was prepared by a solid-state reaction method. Appropriate amounts of $BaCO_3$, ZrO_2 and Y_2O_3 powders were dried at 500–700 °C before mixing together and ball-milling in a zirconia container with zirconia balls. The mixture was then fired at 1400 °C for 10 h. A specific amount of zinc-oxide was mixed together with as-fired powder, ball-milled for 15 min twice, then pressed into pellets in a diameter of 13 mm before firing at 1325 °C. For comparison, pellets pressed from 1400 °C/10 h $BaZr_{0.8}Y_{0.2}O_{3-\delta}$ powder were also fired together at 1325 °C for 10 h with the ones with 1 wt% ZnO additives. In order to determine whether zinc enters the perovskite, a series of $Ba_{0.97}Zr_{0.8}Y_{0.2-x}Zn_xO_{3-\delta}$ samples with x ranging from 0.02 to 0.12 at 0.02 intervals were synthesised by solid-state reaction and fired at 1325 °C for 10 h.

Phase purity and crystal parameters of the samples were examined by X-ray diffraction (XRD) analysis of powders on a Stoe Stadi-P diffractometer. X-POW Software was used to perform least square refinement of the lattice parameters of the samples. Dilatometry of the samples was carried out on a NETZSCH DIL 402C dilatometer (alumina holder) with a TASC 414/4 controller. The micro-structure of the two types of pellets fired at 1325 °C was inspected by scanning electron microscope (SEM) on a JEOL 5600 SEM with a Mica energy dispersive

X-ray spectroscopy (EDS) analysis system. Thermal analysis was carried out on a Rheometric Scientific TG 1000M Plus, and a TA Instruments SDT2960 from room temperature to 900 °C (5 °C/min), holding at 900 °C for 30 min then cooling down to 30 °C (5 °C/min) under flowing wet 5% H_2 in argon at a rate of 20 ml/min. The conductivity of the $Ba_{0.97}Zr_{0.77}Y_{0.19}Zn_{0.04}O_{3-\delta}$ sample was measured by an a.c. method using a Schlumberger Solartron 1255 Frequency Response Analyser coupled with a 1287 Electrochemical Interface controlled by ZPlot and ZView electrochemical impedance software over the frequency range 1 MHz to 100 mHz. The measurements were carried out in air, dry and wet 5% H_2 by passing the gas through 98% H_2SO_4 and room temperature water, respectively. Accordingly, the steam vapour pressure are 8.4×10^{-4}, 1.3×10^{-6} and 3.0×10^{-2} atm for air, dry and wet 5% H_2, respectively [24].

3. Results and discussion

3.1. Sinterability of barium zirconate

Al_2O_3, Bi_2O_3 and some first row transition elements oxides such as TiO_2, Fe_2O_3, CoO, CuO, etc. are commonly used as sintering aids to obtain dense ionic conducting materials such as yttria stabilised zirconia (YSZ) and ceria doped with gadolinia (CGO) [25–28]. The sintering mechanism is generally due to the formation of low melting phases, which lower the sintering temperature. Initial studies indicated that $BaZr_{0.8}Y_{0.2}O_{3-\delta}$ cannot be effectively sintered by addition of these sintering aids at a level of 1 wt%. On the other hand, low melting glasses such as Zn–B–O glass are good low temperature sintering aids [29,30]. The ZnO–B_2O_3 glass was prepared by quenching of the melt of the mixture of ZnO and H_3BO_3 at 1:1 molar ratio from 1000 °C [30]. Pores in the sintered $BaZr_{0.8}Y_{0.2}O_{3-\delta}$ pellets were obviously observed when ZnO–B_2O_3 glass or pure B_2O_3 was used as the sintering aid possibly due to the low melting point (450 °C) and quick evaporation of B_2O_3; however, a dense $BaZr_{0.8}Y_{0.2}O_{3-\delta}$ pellet was obtained when pure ZnO was applied as the sintering aid. To minimise the effect of addition of ZnO on the other properties such as conductivity, a minimum amount of ZnO should be added. In our experiments, it was found that less than 1 wt% of ZnO cannot effectively sinter the $BaZr_{0.8}Y_{0.2}O_{3-\delta}$ pellets. With addition of only 1 wt% ZnO, $BaZr_{0.8}Y_{0.2}O_{3-\delta}$ pellets may be sintered at a temperature as low as 1325 °C. A relative density of 96% was obtained after firing the $BaZr_{0.8}Y_{0.2}O_{3-\delta}$ pellets at 1325 °C for 10 h with addition of 1 wt% ZnO. Possible mechanisms are that ZnO may react with barium oxides to form some intermediate barium zinc oxides which may have relatively lower melting point therefore decreased the sintering temperature of $BaZrO_3$-based perovskite oxides. It has been reported that $BaZnO_2$ may be prepared at a temperature of 1000 °C [31]. Another possibility is that zinc entered the perovskite lattice and the Zn-containing

perovskite exhibits a lower melting point, therefore it is easier to be sintered dense. The ionic size of Zr^{4+} and Zn^{2+} ions are 0.72 and 0.74 Å, respectively [32] which are fairly close. From this point of view, Zn^{2+} ions are easier to enter the $BaZrO_3$ lattice than other transition ions and this could be the reason why zinc is a more effective additive than other transition metal oxides. It is anticipated that oxygen vacancies will be formed when Zr^{4+} ions are replaced by lower valent Zn^{2+} ions which will have an influence on both conduction properties and sintering activity, although as there are already a large number of vacancies in the lattice the effect will be small.

To investigate the sintering process, the 1400 °C/10 h pre-fired $BaZr_{0.8}Y_{0.2}O_{3-\delta}$ powders with and without 1 wt% ZnO sintering aid were pressed into cylinders with 13 mm in diameter and about 10 mm in length. The as-pressed green cylinders were directly put in the sample holder for the sintering shrinkage test without further heat treatment. The samples were heated up at 3 °C/min from room temperature to 1450 °C, held isothermally at 1450 °C for 4 h and cooled down at 3 °C/min to room temperature. The shrinkage behaviour of the two samples is shown in Fig. 1(a). Both samples started shrinking at ~1000 °C, but the one with added ZnO shrank both rapidly and to a greater extent than the pure $BaZr_{0.8}Y_{0.2}O_{3-\delta}$ sample

particularly at the isothermal stage. The total shrinkage of the ZnO added sample was 15.17% which is about 8.6 times of that of $BaZr_{0.8}Y_{0.2}O_{3-\delta}$ (1.76%). Fig. 1(b) plots the shrinkage over time which clearly shows that minor shrinkage was observed for $BaZr_{0.8}Y_{0.2}O_{3-\delta}$ sample. The effect of ZnO addition on sintering is significant.

Scanning electron microscopy was applied to observe the microstructure of the sintered samples. The picture clearly shows that the $BaZr_{0.8}Y_{0.2}O_{3-\delta}$ (BZY) pellet without ZnO addition is quite porous after firing at 1325 °C. The relative density of the sample is only ~68% (Fig. 2(a)) calculated from an estimated theoretical density using the lattice parameters from XRD data (Fig. 3). On the contrary, the relative density of the ZnO added sample reached 96% (Fig. 2(b)). $BaZr_{0.8}Y_{0.2}O_{3-\delta}$ is therefore successfully sintered at 1325 °C with the addition of only 1 wt% ZnO (BZYZn). EDS analysis indicates that zinc was homogeneously distributed in the sample (Fig. 2(c)) which is consistent with the XRD results. It should be noted that the BZY pellets cracked into powders after exposing to laboratory air for a couple of days; however, the BZYZn pellets kept their shape even after exposing to air for over a year. This may arise from the enhanced density and the reduction in extent of grain-boundary regions, although it may also relate to enhanced chemical stability. It was reported that BZY samples with a little barium excess exhibit higher conductivity [18] but in our experiments, all the barium excess BZY samples (up to 20% Ba excess) cracked into powders relatively quicker after exposure to air. Therefore, it could be difficult to use BZY compositions with excess barium at the A-site.

3.2. Composition and structure of sintered barium zirconate

The nominal $BaZr_{0.8}Y_{0.2}O_{3-\delta}$ sample after the firing process contains three phases indicating that equilibrium had not been attained at this temperature (Fig. 3(a)). There are two cubic phases with lattice parameters $a = 4.2292(9)$ Å (phase A) and 4.1955(5) Å (phase B), respectively. Pure $BaZrO_3$ exhibits a cubic structure with a lattice parameter $a = 4.193$ Å (ICPDS 6-399) which is very close to that of phase B. $BaZr_{0.95}Y_{0.05}O_{3-\delta}$ exhibits a cubic structure with $a = 4.2058(1)$ Å [16] which is fairly close to that of phase A. The symmetry is reported to decrease to tetragonal when yttria content reaches 10% at the B-site [16] indicating that phase B is a doped barium zirconate $BaZr_{1-x}Y_xO_{3-\delta}$ with $0.05 < x < 0.1$. The molar ratio of phase A to B is roughly 50:50 according to the relative intensities of the strongest (110) diffraction. The peak at $d = 3.0265$ Å with relative intensity ~11% may not be indexed by these two phases which could be the strongest (111) diffraction of Y_2O_3 (ICPDS card 43-661) or (101) of tetragonal yttrium stabilised zirconia (YSZ) (ICPDS card 42-1164) indicating the presence of Y_2O_3 and/ or YSZ (phase C) in the mixture. It was confirmed that this is YSZ rather than pure Y_2O_3 by EDS point element analysis under SEM observation. The presence of YSZ in
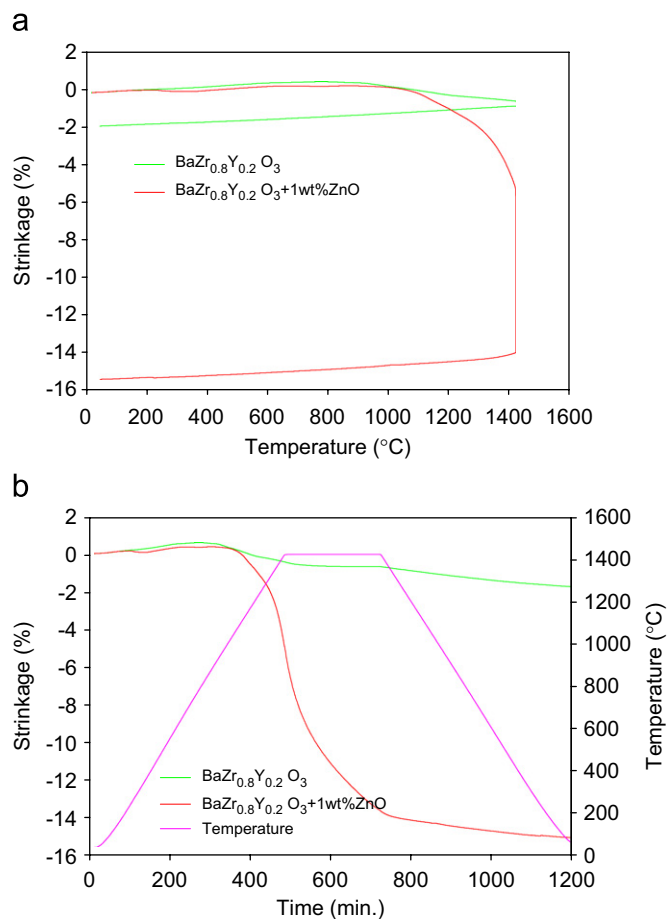

Fig. 1. The shrinkage of the green $BaZr_{0.8}Y_{0.2}O_{3-\delta}$ cylinder with and without ZnO additive as a function of firing temperature (a) and time (b).
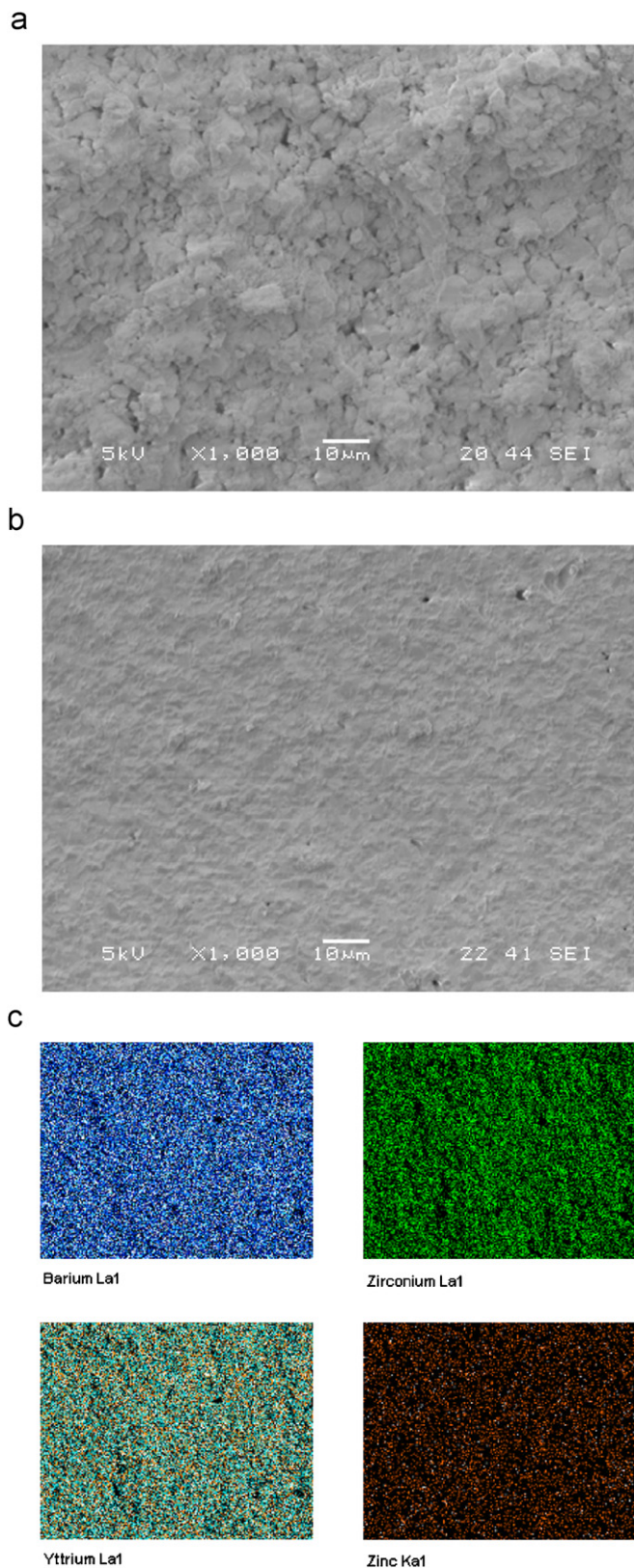
a

b

c

Barium La1

Zirconium La1

Yttrium La1

Zinc Ka1

Fig. 2. SEM cross section of $BaZr_{0.8}Y_{0.2}O_{3-\delta}$ pellets (a) calcined at 1400 °C/10 h, then pressed into a pellet, fired at 1325 °C/10 h, (b) pellet formed from 1 wt% ZnO added to 1400 °C powder and fired at 1325 °C/ 10 h, (c) EDS elemental mapping of the ZnO added sample shown in (b).
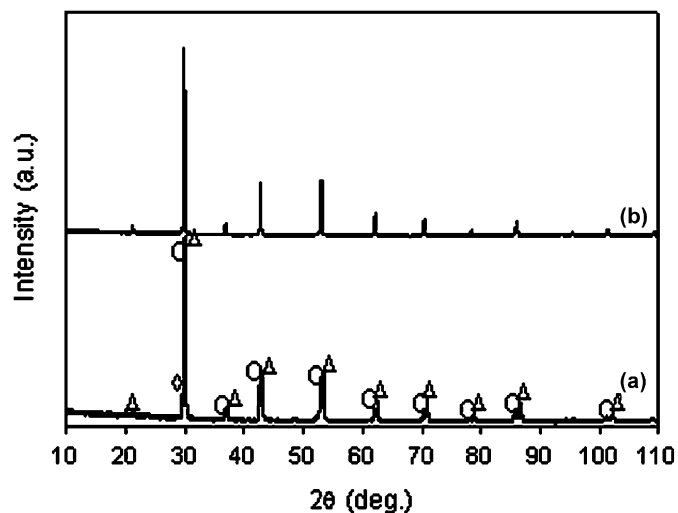

Fig. 3. The X-ray diffraction pattern of sintered $BaZr_{0.8}Y_{0.2}O_{3-\delta}$ cylinder without (a) and with (b) ZnO additive: O, phase A; Δ, phase B; $\diamond$, YSZ.

the $BaZr_{1-x}Y_xO_{3-\delta}$ perovskite oxides was also observed by other authors firing at a higher temperature [7] which was attributed to the evaporation of some BaO on firing. The YSZ impurity was also observed in the $Ba_{1+x}Zr_{0.8}Y_{0.2}O_{3\pm\delta}$ ($x \leqslant 0.2$) samples indicating that in this study, this is more likely due to the incomplete reaction. In brief, the nominal $BaZr_{0.8}Y_{0.2}O_{3-\delta}$ fired at 1400 °C seems to be a mixture of $BaZrO_3$, Y-doped $BaZrO_3$, and YSZ. Increasing the firing temperature to 1600 °C does not help phase formation. Under these circumstances, similar composition was observed except that the relative intensity of phase C decreases a little. In our experiments, single phase $BaZr_{0.8}Y_{0.2}O_{3-\delta}$ was not obtained by firing the pellets pressed from the 1400 °C pre-fired powders at 1700 °C for 10 h under vacuum although the pellets were buried in $BaZrO_3$ to avoid the evaporation of BaO. Therefore, as reported, a firing temperature higher than 1600 °C, say 1700 °C, is required to obtain a single phase $BaZr_{0.8}Y_{0.2}O_{3-\delta}$ when prepared by solid state reaction, although it was not obtained even at 1700 °C in our experiments. On the contrary, the sample with 1 wt% ZnO sintering aid fired at 1325 °C is a single phase and well crystallised (Fig. 3(b)), roughly 350 °C lower than that required for pure $BaZr_{0.8}Y_{0.2}O_{3-\delta}$.

The homogeneous distribution of zinc in the BZYZn sample indicates that zinc did enter the bulk rather stay at the grain boundary as is the usual for sintering aids. In order to further confirm this, a series of samples with nominal formula $Ba_{0.97}Zr_{0.8}Y_{0.2-x}Zn_xO_{3-\delta}$ ranging from $x = 0.02$ to 0.12 with 0.02 interval were synthesised, such A-site deficiency is often utilised to avoid BaO rich grain boundary regions. The XRD patterns of these materials are shown in Figs. 4 and 5. The phase composition and lattice parameters of those phases are listed in Table 1 as well. The phase composition of $Ba_{0.97}Zr_{0.8}Y_{0.18}Zn_{0.02}O_{3-\delta}$ is similar to $BaZr_{0.8}Y_{0.2}O_{3-\delta}$ indicating that low level doping cannot effectively improve the formation of the perovskite single
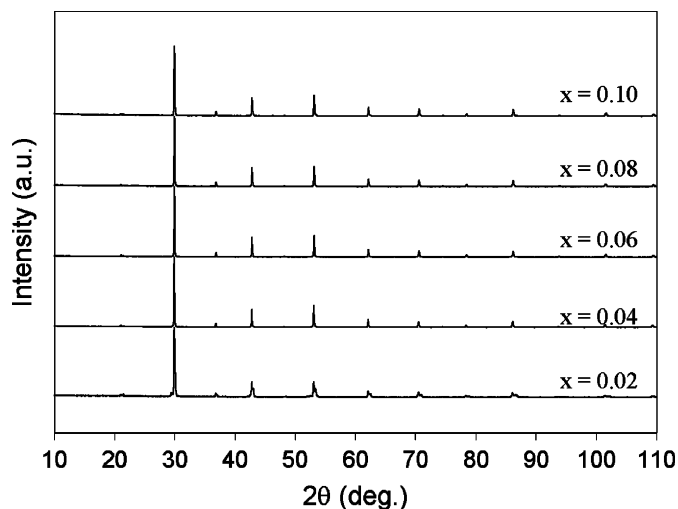
Fig. 4. XRD powder pattern of "$Ba_{0.97}Zr_{0.8}Y_{0.2-x}Zn_xO_{3-\delta}$" series with different zinc content.

Fig. 5. XRD powder pattern of $Ba_{0.97}Zr_{0.8}Y_{0.08}Zn_{0.12}O_{3-\delta}$. * Unidentified peaks.

Table 1
Lattice parameters of $Ba_{0.97}Zr_{0.8}Y_{0.2-x}Zn_xO_{3-\delta}$ sample fired at 1325 °C for 10 h

Nominal composition	Lattice parameters of phases	Note
$BaZr_{0.8}Y_{0.2}O_{3-\delta}$	Phase A: $a = 4.2292(9)$ Å, $V = 75.64(5)$ Å^3	Containing trace $Zr_{1-x}Y_xO_y$ phase
	Phase B: $a = 4.1955(5)$ Å, $V = 73.85(2)$ Å^3	
$Ba_{0.97}Zr_{0.8}Y_{0.18}Zn_{0.02}O_{3-\delta}$	Phase A: $a = 4.2217(10)$ Å, $V = 75.24(3)$ Å^3	Containing trace $Zr_{1-x}Y_xO_y$ phase
	Phase B: $a = 4.1995(5)$ Å, $V = 74.06(4)$ Å^3	
$Ba_{0.97}Zr_{0.8}Y_{0.16}Zn_{0.04}O_{3-\delta}$	$a = 4.2220(4)$ Å, $V = 75.26(1)$ Å^3	Single phase
$Ba_{0.97}Zr_{0.8}Y_{0.14}Zn_{0.06}O_{3-\delta}$	$a = 4.2189(3)$ Å, $V = 75.09(1)$ Å^3	Single phase
$Ba_{0.97}Zr_{0.8}Y_{0.12}Zn_{0.08}O_{3-\delta}$	$a = 4.2189(4)$ Å, $V = 75.09(1)$ Å^3	Containing second phase(s)
$Ba_{0.97}Zr_{0.8}Y_{0.10}Zn_{0.10}O_{3-\delta}$	$a = 4.2171(3)$ Å, $V = 74.99(1)$ Å^3	Containing second phase(s)
$Ba_{0.97}Zr_{0.8}Y_{0.08}Zn_{0.12}O_{3-\delta}$	$a = 4.2161(4)$ Å, $V = 74.70(1)$ Å^3	Containing second phase(s)

For comparison, Zn-free $BaZr_{0.8}Y_{0.2}O_{3-\delta}$ fired at 1400 °C for 10 h is also listed together.

$Ba_{0.97}Zr_{0.8}Y_{0.2-x}Zn_xO_{3-\delta}$ indicates that zinc enters the perovskite lattice rather than remaining at the grain surface. Obviously if excess ZnO is utilised not all can be accommodated in the lattice and it is also possible that reaction between the lattice and ZnO may not be complete, both of which would leave some ZnO at the grain boundary.

Further increasing the Zn content at the B-site leads to the appearance of some weak impurity peaks. As shown in Fig. 5, weak unidentified peaks were observed which do not belong to the perovskite phase also they cannot be indexed by any known compounds composed of Ba, Zr, Y, Zn and O. Also they cannot be indexed by perovskite lattice with lower symmetry and reasonable larger unit cell. Further investigation is required to identify the second phases. The lattice parameters of the main phase with nominal composition $Ba_{0.97}Zr_{0.8}Y_{0.12}Zn_{0.08}O_{3-\delta}$ is nearly identical to that of $Ba_{0.97}Zr_{0.8}Y_{0.14}Zn_{0.06}O_{3-\delta}$ indicating that limit of zinc for solid solution is $x = 0.06$ in the $Ba_{0.97}Zr_{0.8}Y_{0.2-x}Zn_xO_{3-\delta}$ series. The lattice parameters of the main perovskite phase decrease with zinc content higher than 0.08 indicating the formation of Zn-rich perovskite phases but accordingly the intensity of second phase also increases. Therefore, the formation of single-phase perovskite phase in the $Ba_{0.97}Zr_{0.8}Y_{0.2-x}Zn_xO_{3-\delta}$ series locates at $x = 0.04$–0.06.

The main focus of the conductivity studies in this paper relates to a composition slightly richer in yttria than those detailed above, $Ba_{0.97}Zr_{0.77}Y_{0.19}Zn_{0.04}O_{3-\delta}$. On careful inspection of the XRD pattern some small addition peaks and broadening are observed, indicting that the additional

phase. However, a single cubic perovskite phase formed when zinc at the B-site increases to 0.04 (~1 wt% ZnO). The material with nominal composition $Ba_{0.97}Zr_{0.8}Y_{0.14}Zn_{0.06}O_{3-\delta}$ is also a single phase but the lattice parameter is slightly smaller than that of $Ba_{0.97}Zr_{0.8}Y_{0.16}Zn_{0.04}O_{3-\delta}$. The ionic sizes of Zr^{4+}, Y^{3+} and Zn^{2+} at six-coordination are 0.72, 0.90 and 0.74 Å, respectively [32]. It is expected that the lattice parameter will decrease with the replacement of Y^{3+} ions by the smaller Zn^{2+}. On the other hand, the formation of more oxygen vacancies might give rise to lattice expansion with the loss of negatively charged oxygen weakening the extent of ionic bonding. It seems likely that zinc enters the B-site of the perovskite rather than staying in the grain boundary from both XRD and EDS analysis. It was reported that zinc accumulates at the grain boundary in the yttrium-doped $BaZrO_3$ sample [23]. The difference could be due to variations in the experimental process or the slight difference in the composition. In our experiments, the obvious lattice parameter change in the

large yttrium ion in the lattice distorts it from cubic. Structure refinement was performed by the Rietveld method using the program General Structure Analysis System (GSAS) [33]. The ionic size of Zn^{2+} (0.74 Å) is too small for these ions to enter the A-site. It is supposed that zinc goes to the B-sites on firing therefore the formula of the $BaZr_{0.8}Y_{0.2}O_{3-\delta}$ sample with 1 wt% ZnO sintering aid may be written as $Ba_{0.97}Zr_{0.77}Y_{0.19}Zn_{0.04}O_{3-\delta}$ assuming the evaporation of BaO and ZnO is negligible at the given temperature. The best refinement result was achieved for a tetragonal structure with space group $P4/mbm$ (127); $a = 5.9787(1)$ Å, $c = 4.2345(1)$ Å, $V = 151.36(1)$ Å^3 ($\chi^2_{red} = 1.833$). The observed, calculated and difference profiles for the refinement of $Ba_{0.97}Zr_{0.77}Y_{0.19}Zn_{0.04}O_{3-\delta}$ are shown in Fig. 6. The final refined structural data are given in Table 2. Another common tetragonal perovskite structure is space group $I4/mcm$ (140) with lattice parameters $\sqrt{2}a \times \sqrt{2}a \times 2a$ where a ≈ 4 Å which is the parameter of primitive cubic perovskite [34]. The R_{wp} (13.94%), R_p (10.15%) and goodness-of-fit value (2.491) is much larger than that for $P4/mbm$ (127) (Table 2). Therefore, $P4/mbm$ (127) with $\sqrt{2}a \times \sqrt{2}a \times a$ is likely to be the right structure for $Ba_{0.97}Zr_{0.77}Y_{0.19}Zn_{0.04}O_{3-\delta}$. The same space group has been reported for the closely related composition $BaCe_{0.95}Nd_{0.05}O_{3-\delta}$ [35].

It should be noted that structure of perovskite oxides is very sensitive to their composition. The structure of $Ba_{0.97}Zr_{0.8}Y_{0.16}Zn_{0.04}O_{3-\delta}$ is primitive cubic, but the one with a little more yttrium in the B-site, $Ba_{0.97}Zr_{0.77}Y_{0.19}Zn_{0.04}O_{3-\delta}$ is tetragonal. Pure $BaZrO_3$ is a primitive cubic perovskite. With the introduction of large Y^{3+} ions at the B-sites, the BO_6 polyhedra may tilt and distort thus cause distortion of the lattice. Therefore, it is expected that the more yttrium in the lattice, the more likely to go to lower symmetry.

TGA analyses were carried out in wet 5% H_2 on a freshly dried $Ba_{0.97}Zr_{0.77}Y_{0.19}Zn_{0.04}O_{3-\delta}$ powder sample (900 °C in air) and a powder sample stored at ambient atmosphere for over a year. Significant water loss was observed for both samples starting at temperatures over 350 °C and continuing to 900 °C. More weight loss was observed for the stored sample (1.2 wt%) than the freshly dried sample (0.8 wt%), reflecting the very slow rate of water uptake.

3.3. Conductivity of doped barium zirconate samples

Fig. 7 shows the bulk, grain and total conductivity for $BaZr_{0.8}Y_{0.2}O_{3-\delta}$ as a function of temperature in different atmospheres. Bulk and grain boundary elements show classical pF cm^{-1} and nF cm^{-1} geometric capacitance values. In air, the bulk and grain boundary parts cannot be separated below 450 °C. The grain boundary conductivity is higher than that of the bulk above 550 °C. The conductivity in dry 5% H_2 (Fig. 7(b)) is significantly lower

Table 2
Structure parameters of $Ba_{0.97}Zr_{0.77}Y_{0.19}Zn_{0.04}O_{3-\delta}$ obtained at 1325 °C from X-ray diffraction data

Atom	Site	Occupancy	x	y	z	U_{iso} (Å^2)
Ba	2c	0.97	0	0.5	0.5	0.0124(6)
Zr	2a	0.77	0	0	0	0.0082(7)
Y	2a	0.19	0	0	0	0.0082(7)
Zn	2a	0.04	0	0	0	0.0082(7)
O(1)	2b	1	0	0	0.5	0.0198(15)
O(2)	4g	1	0.276(3)	0.224(3)	0	0.0198(15)

Note: Space group $P4/mbm$ (127); $a = 5.9787(1)$ Å, $c = 4.2345(1)$ Å, $V = 151.36(1)$ Å^3, $Z = 2$. $R_{wp} = 11.95\%$, $R_p = 8.99\%$, $\chi^2_{red} = 1.833$.
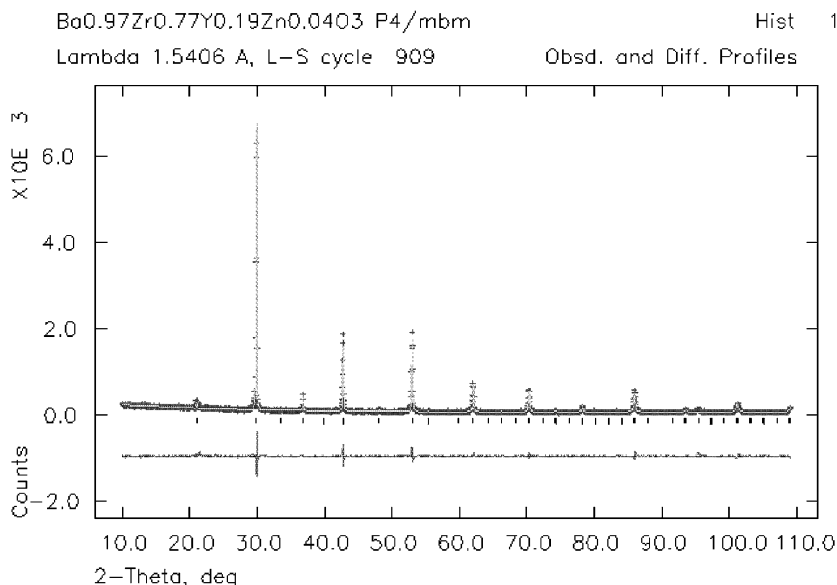

Fig. 6. X-ray diffraction of $Ba_{0.97}Zr_{0.77}Y_{0.19}Zn_{0.04}O_{3-\delta}$ formed at 1325 °C. Upper: experimental (crosses) and calculated (line); lower: residual.
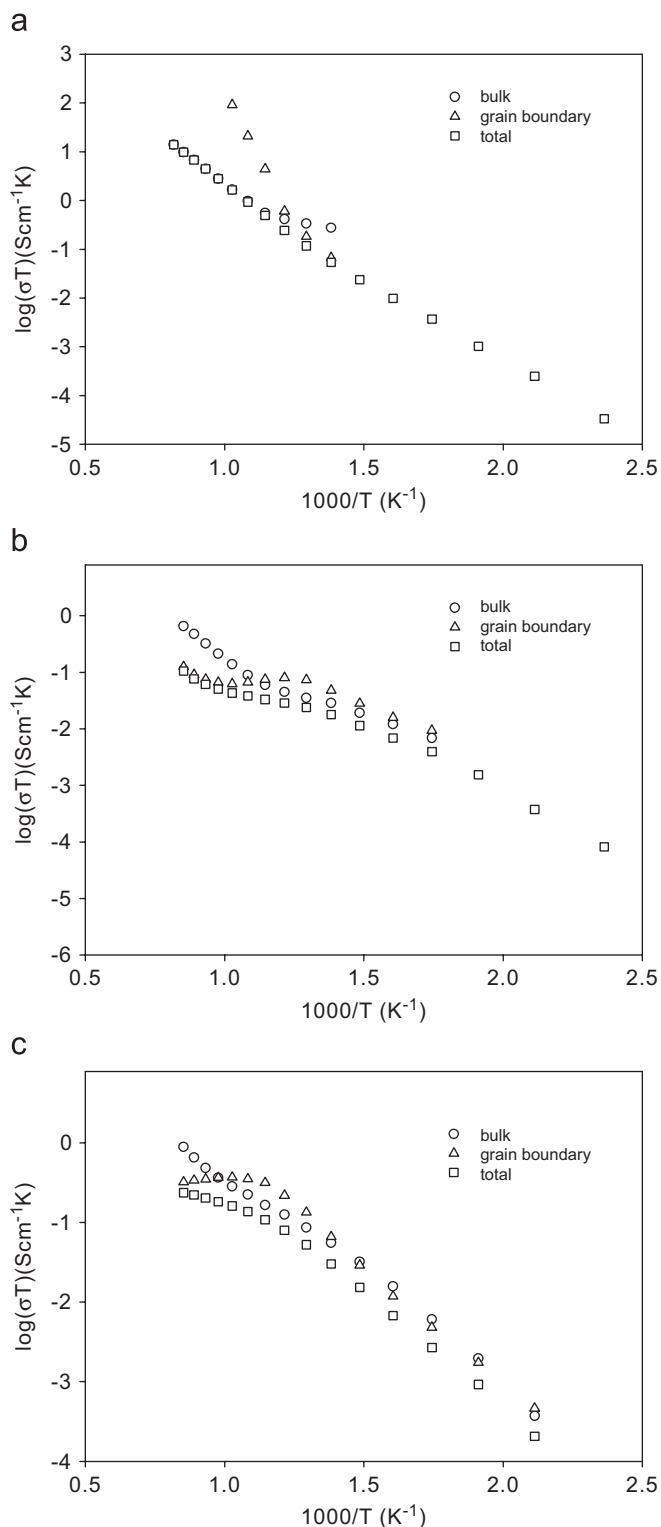
a

b

c

Fig. 7. Conductivity of $BaZr_{0.8}Y_{0.2}O_{3-\delta}$ in air (a), dry 5% H_2 (b) and wet 5% H_2 (c). Sample sintered at 1325 °C without additives.

than in air. At 600 °C, the bulk and grain boundary conductivity are comparable, but the grain boundary conductivity is lower than the bulk above 650 °C. The grain boundary dominated total conductivity. It is only 9.0×10^{-5} S/cm at 900 °C which is more than two orders of

magnitude lower than that in air (1.14×10^{-2} S/cm) at the same temperature. The conductivity of the $BaZr_{0.8}Y_{0.2}O_{3-\delta}$ sample in wet 5% H_2 is plotted in Fig. 7(c). Similar to dry 5% H_2, the total resistivity is dominated by the grain boundary above 750 °C. The grain boundary resistance is less than the bulk below 750 °C due to the absorption of steam, which leads to proton conduction. The bulk, grain boundary and total conductivities after equilibrating in wet 5% H_2 are all higher than those in dry 5% H_2 or on heating in wet 5% H_2 before water equilibration has occurred, indicating that the significant improvement in conductivity is due to the absorption of steam resulting in enhanced proton conduction. The total conductivity in wet 5% H_2 at 900 °C is 2.02×10^{-4} S/cm which is twice of that in dry 5% H_2. The grain boundary conductivity of $BaZr_{0.8}Y_{0.2}O_{3-\delta}$ at 500 °C is 2.35×10^{-4}, 9.54×10^{-5} and 1.74×10^{-4} S/cm in air, dry 5% H_2 and wet 5% H_2, respectively.

Conductivity measurements on $Ba_{0.97}Zr_{0.77}Y_{0.19}Zn_{0.04}O_{3-\delta}$ also sintered at 1325 °C are presented in Fig. 8. As shown in Fig. 8(a), the total conductivity in air is dominated by grain boundary only up to 400 °C. The contribution from grain boundary at the working temperature (usually above 450 °C) is negligible. The total conductivity at 900 °C is 1.94×10^{-2} S/cm which is nearly double that of $BaZr_{0.8}Y_{0.2}O_{3-\delta}$ under the same condition. When switching from air to dry 5% H_2 at 900 °C, it was found that conductivity of the $Ba_{0.97}Zr_{0.77}Y_{0.19}Zn_{0.04}O_{3-\delta}$ sample decreased with time possibly due to a combination of loss of p-type conduction on reduction and loss of protonic contribution on dehydration. The p-type conduction of Y-doped $BaZrO_3$ at higher pO_2 is well known [36] and it is reasonable to assume that $Ba_{0.97}Zr_{0.77}Y_{0.19}Zn_{0.04}O_{3-\delta}$ also exhibits a similar behaviour. As shown in Fig. 9, the conductivity became relatively stable after ageing in dry 5% H_2 for 150 min, with both bulk and grain boundary equilibrating over the same timescale. After ageing in 5% H_2 at 900 °C for 60 h, the conductivity in 5% H_2 was measured on cooling. As shown in Fig. 8(b), the bulk and grain boundary conductivities are comparable at 400 °C. The total conductivity is bulk-dominated above 500 °C.

The change in bulk, grain boundary and total conductivity with time of $Ba_{0.97}Zr_{0.77}Y_{0.19}Zn_{0.04}O_{3-\delta}$ on changing from dry to wet 5% H_2 at 350 °C, at time = 0, is shown in Fig. 10. The bulk conductivity remains almost constant over 2 days but the grain boundary conductivity keeps increasing during the first 25 h except for the initial decrease, which is probably due to temperature fluctuation. As can be seen in Fig. 10, the bulk remains at the dry value indicating that water diffusion through the bulk is very slow, whilst the grain boundary is more responsive but still quite slow.

After holding in wet 5% H_2 at 350 °C for 48 h, the conductivity of $Ba_{0.97}Zr_{0.77}Y_{0.19}Zn_{0.04}O_{3-\delta}$ was measured on both heating and cooling in wet 5% H_2. The heating curve for the bulk was very close to that measured in dry 5% H_2 up to 500 °C with converged behaviour from 650 upwards, Fig. 11. The grain boundary conductivities on
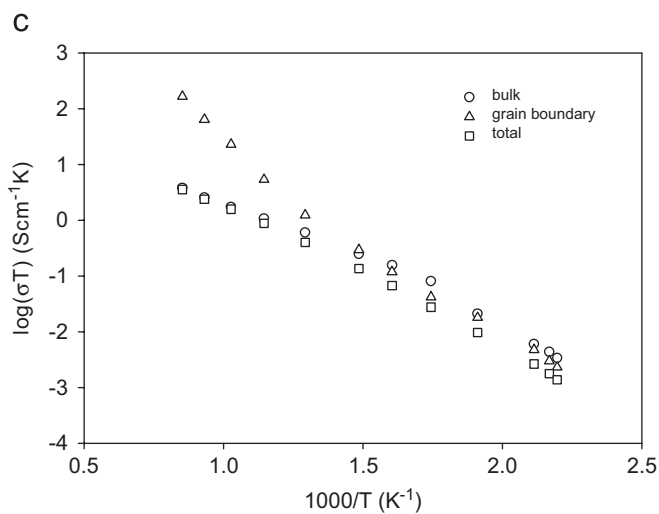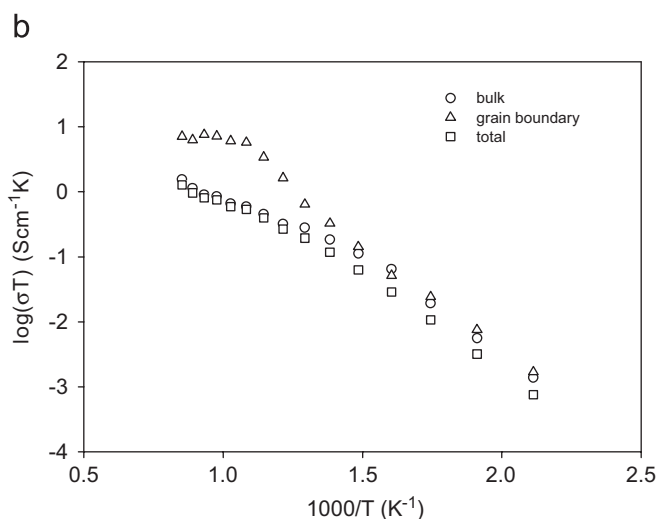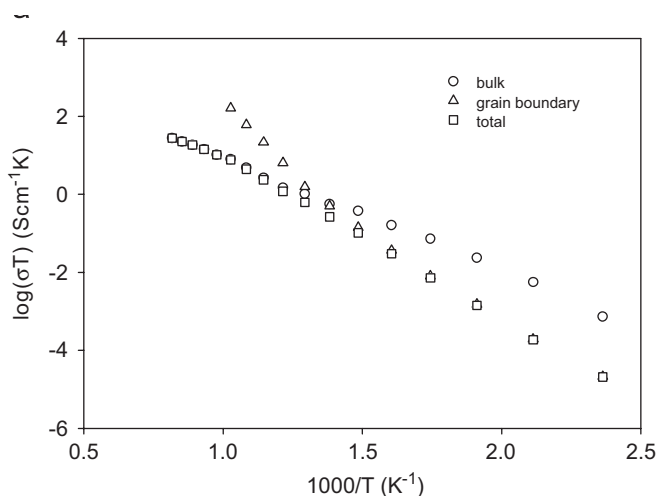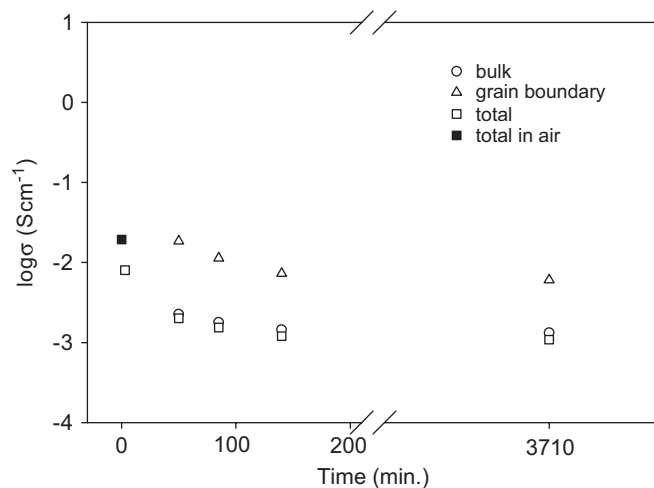
Fig. 9. The conductivity change with time of $Ba_{0.97}Zr_{0.77}Y_{0.19}Zn_{0.04}O_{3-\delta}$ in dry 5% H_2 at 900 °C on switching atmosphere from air at 900 °C.

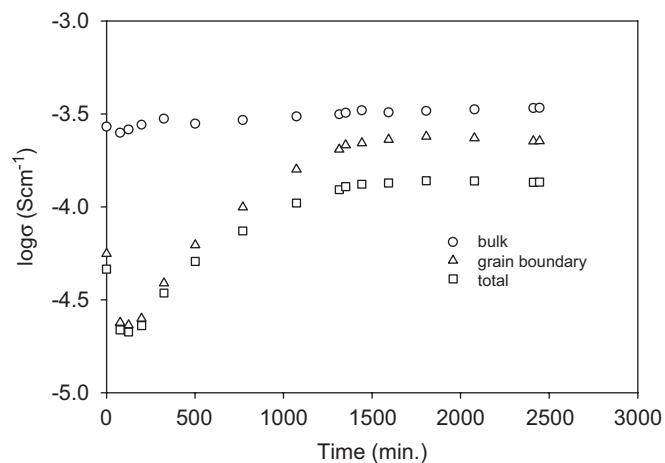Fig. 10. The conductivity change with time of $Ba_{0.97}Zr_{0.77}Y_{0.19}Zn_{0.04}O_{3-\delta}$ in wet 5% H_2 at 350 °C on changing from dry to wet (3% H_2O).

Fig. 8. Conductivity of $Ba_{0.97}Zr_{0.77}Y_{0.19}Zn_{0.04}O_{3-\delta}$ in air (a), dry 5% H_2 (b) and wet 5% H_2 (c). Sample sintered at 1325 °C.
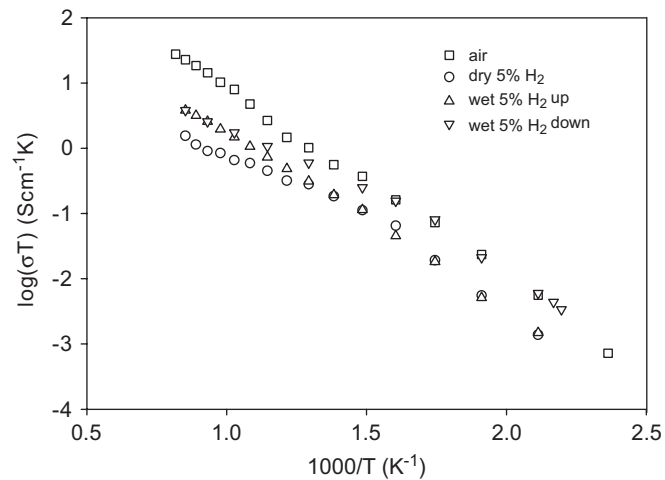

Fig. 11. Comparison of bulk conductivity of $Ba_{0.97}Zr_{0.77}Y_{0.19}Zn_{0.04}O_{3-\delta}$ in different atmospheres.

heating and cooling were essentially identical, following equilibration at 350 °C. The total conductivities in wet 5% H_2 at 600 °C and 900 °C are 1.01×10^{-3} and 3.02×10^{-3} S/cm, respectively. $Ba_{0.97}Zr_{0.77}Y_{0.19}Zn_{0.04}O_{3-\delta}$ may be

therefore used as the electrolyte above 600 °C if thin film technology is applied.

Fig. 11 shows the bulk conductivities of the $Ba_{0.97}Zr_{0.77}Y_{0.19}Zn_{0.04}O_{3-\delta}$ in different atmospheres. Data for air and dry 5% H_2 were collected on cooling. The bulk conductivity in air is the highest. Below 450 °C, the conductivity in air and wet 5% H_2 on cooling are comparable. High grain boundary conductivity was observed in air above 450 °C (Fig. 12). The grain boundary conductivity in dry 5% H_2 is the lowest at high temperature. The grain boundary conductivity was higher in wet 5% H_2 than in dry 5% H_2 indicating proton conduction. The total conductivities of $Ba_{0.97}Zr_{0.77}Y_{0.19}Zn_{0.04}O_{3-\delta}$ in different atmospheres are shown in Fig. 13. From the impedance data in Fig. 14 at 200 °C, it is clear that $Ba_{0.97}Zr_{0.77}Y_{0.19}Zn_{0.04}O_{3-\delta}$ exhibits the highest conductivity in wet 5% H_2 below 500 °C, strongly indicating
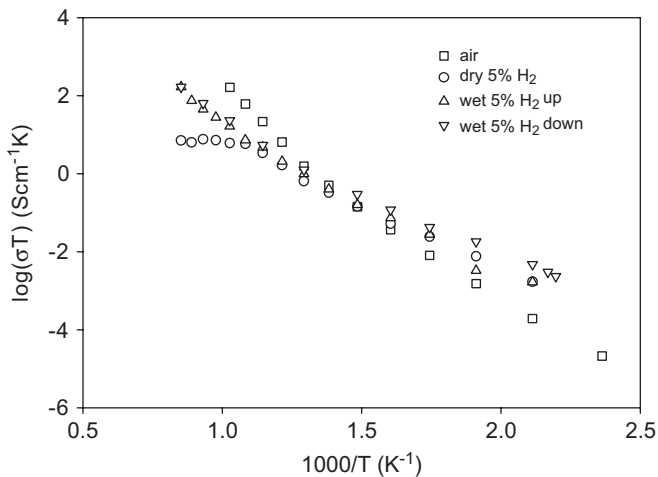

Fig. 14. A.c. impedance of $Ba_{0.97}Zr_{0.77}Y_{0.19}Zn_{0.04}O_{3-\delta}$ at 200°C in different atmospheres: □, in air; ○, in dry 5% H_2; Δ, in wet 5% H_2.

Fig. 12. Comparison of grain boundary conductivity of $Ba_{0.97}Zr_{0.77}Y_{0.19}Zn_{0.04}O_{3-\delta}$ in different atmospheres.
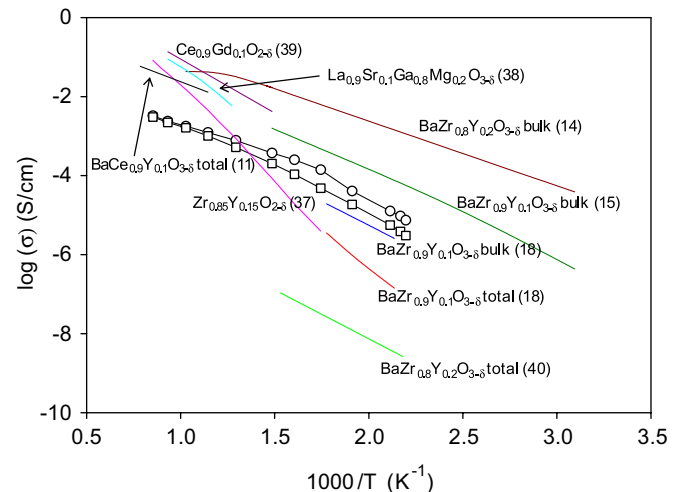
Fig. 15. Conductivity versus reciprocal temperature for selected solid oxide electrolytes: (□) total; (○) bulk for $Ba_{0.97}Zr_{0.77}Y_{0.19}Zn_{0.04}O_{3-\delta}$.

proton conduction. A large grain boundary response was observed in air at 200 °C, which was observed by other authors as well [7,15]. However, the grain boundary response in dry 5% H_2 is comparable to that of the bulk. For comparison, the conductivities of the samples with and without ZnO addition in different atmospheres are shown together in Fig. 13. In general, the well-sintered sample $Ba_{0.97}Zr_{0.77}Y_{0.19}Zn_{0.04}O_{3-\delta}$ exhibits much higher conductivity than the less dense $BaZr_{0.8}Y_{0.2}O_{3-\delta}$ under the same conditions.

The bulk and total conductivity of $Ba_{0.97}Zr_{0.77}Y_{0.19}Zn_{0.04}O_{3-\delta}$ in wet 5% H_2 are plotted together with other ionic conductors (Fig. 15). The conductivities of $BaZr_{0.8}Y_{0.2}O_{3-\delta}$ and $BaZr_{0.9}Y_{0.1}O_{3-\delta}$ from different reports are plotted as well. Some typical oxygen ion and
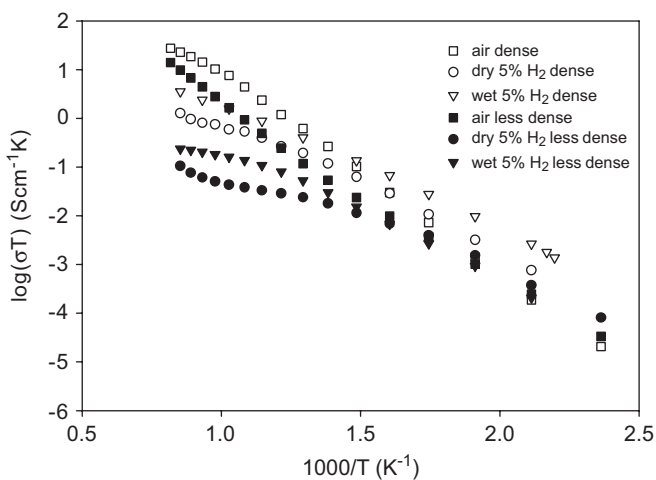

Fig. 13. Comparison of total conductivity of $Ba_{0.97}Zr_{0.77}Y_{0.19}Zn_{0.04}O_{3-\delta}$ and the less dense $BaZr_{0.8}Y_{0.2}O_{3-\delta}$ in different atmospheres, both sintered at 1325 °C.
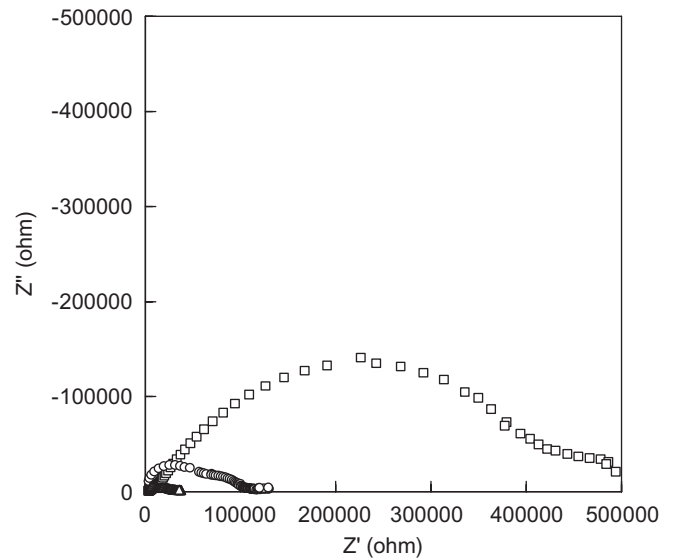
proton conductors are also plotted for comparison [37–39]. The total and bulk conductivity of $Ba_{0.97}Zr_{0.77}Y_{0.19}Zn_{0.04}O_{3-\delta}$ is rather close indicating that the contribution of grain boundary to the total resistance is not very high for the well-sintered sample. The bulk conductivity for $Ba_{0.97}Zr_{0.77}Y_{0.19}Zn_{0.04}O_{3-\delta}$ is slightly lower than that reported for $BaZr_{0.9}Y_{0.1}O_{3-\delta}$ [15] but much lower than that of $BaZr_{0.8}Y_{0.2}O_{3-\delta}$ [16]; however, the total conductivity is much higher than that reported by Snijkers [18] and Schneller [40] for $BaZr_{0.9}Y_{0.1}O_{3-\delta}$. The conductivity of the $BaZrO_3$-based proton conductor strongly depends upon synthesis and measuring conditions. High total conductivity is desired for the electrolyte of any practical electrochemical cell. From this point of view, $Ba_{0.97}Zr_{0.77}Y_{0.19}Zn_{0.04}O_{3-\delta}$ exhibits the highest total proton conductivity among the stable materials. Its total conductivity reached 1.01×10^{-3} S/cm at 600 °C and 3.02×10^{-3} S/cm at 900 °C. At 600 °C, the resistance of the $Ba_{0.97}Zr_{0.77}Y_{0.19}Zn_{0.04}O_{3-\delta}$ electrolyte would be less than $0.2\,\Omega$ for a thin film electrolyte with a thickness of $2\,\mu m$ [41].

4. Conclusion

The $BaZrO_3$-based material $BaZr_{0.8}Y_{0.2}O_{3-\delta}$ has been successfully densified at 1325 °C by adding 1 wt% sintering aid ZnO. This temperature is significantly lower than the required sintering temperature 1700 °C without additive which given the fact that $Ba(Zr_{0.50}Ti_{0.50})O_3$ thin films have been prepared by a polymeric precursor method [42], opens the door to the possibility to fabricating thin films of the materials onto suitable electrode materials. The relatively densities of the $BaZr_{0.8}Y_{0.2}O_{3-\delta}$ sample with and without ZnO additive are 68% and 96%, respectively, under the same sintering temperature 1325 °C. The $BaZrO_3$-based proton conductor is therefore effectively sintered at a much lower temperature. ZnO addition also significantly enhances ease of single-phase formation.

It is observed that zinc enters the lattice on firing from both EDS and XRD analyses forming a solid solution with the Zn expected to occupy the B-site. The formula of the sample with ZnO sintering aid may be written as $Ba_{0.97}Zr_{0.77}Y_{0.19}Zn_{0.04}O_{3-\delta}$. The sample is a single phase and exhibits a tetragonal structure with space group $P4/mbm$ (127); $a = 5.9787(1)$ Å, $c = 4.2345(1)$ Å, $V = 151.36(1)$ Å^3.

The conductivity of the well-sintered sample is much higher than the less dense sample as expected. In general, the conductivity in wet 5% H_2 is higher than that in dry 5% H_2 indicating proton conduction. At low temperature, the proton conduction is limited by the grain boundary rather than the bulk. At high temperature, both bulk and grain boundary conductivities are improved in the presence of steam. The grain boundary resistance is insignificant at high temperature for the well-sintered sample. The total conductivity of $Ba_{0.97}Zr_{0.77}Y_{0.19}Zn_{0.04}O_{3-\delta}$ reaches 1.0×10^{-3} S/cm above 600 °C therefore it may be used as

proton-conducting electrolyte for electrochemical devices with the application of thin film.

References

[1] H. Iwahara, T. Esaka, H. Uchida, N. Maeda, Solid State Ionics 3–4 (1981) 359.
[2] N. Bonanos, K.S. Knight, B. Ellis, Solid State Ionics 79 (1995) 161.
[3] H. Iwahara, Solid State Ionics 86 (9) (1996) 9.
[4] K.D. Kreuer, Chem. Mater. 8 (1996) 610.
[5] K.D. Kreuer, Solid State Ionics 97 (1997) 1.
[6] T. Norby, Solid State Ionics 125 (1999) 1.
[7] K.D. Kreuer, Annu. Rev. Mater. Res. 33 (2003) 333.
[8] F.L. Chen, O.T. Sorensen, G.Y. Meng, D.K. Peng, J. Mater. Chem. 7 (1997) 481.
[9] S.V. Bhide, A.V. Virkar, J. Electrochem. Soc. 146 (1999) 2038.
[10] K.H. Ryu, S.M. Haile, Solid State Ionics 125 (1999) 355.
[11] K. Katahira, Y. Kohchi, T. Shimura, H. Iwahara, Solid State Ionics 138 (2000) 91.
[12] T. Hibino, A. Hashimoto, M. Suzuki, M. Sano, J. Electrochem. Soc. 149 (2002) A1503.
[13] F. Iguchi, N. Sata, T. Tsurui, H. Yugami, Solid State Ionics 178 (2007) 691.
[14] K.D. Kreuer, Solid State Ionics 125 (1999) 285.
[15] H.G. Bohn, T. Schober, J. Am. Ceram. Soc. 83 (2000) 768.
[16] K.D. Kreuer, S. Adams, W. Munch, A. Fuchs, U. Klock, J. Maier, Solid State Ionics 145 (2001) 295.
[17] M. Laidoudi, I. Abu Talib, R. Omar, J. Phys. D: Appl. Phys. 35 (2002) 397.
[18] F.M.M. Snijkers, A. Buekenhoudt, J. Cooymans, J.J. Luyten, Scr. Mater. 50 (2004) 655.
[19] A.M. Azad, S. Subramaniam, T.W. Dung, J. Alloys Compds. 334 (2002) 118.
[20] J.R. Tolchard, T. Grande, Solid State Ionics 178 (2007) 593.
[21] J.T.S. Irvine, S.W. Tao, C. D. Savaniu, A. Kruth, British Patent Application, No. 0406818.5; European Patent Application No. 03766465.3, 2004.
[22] S.W. Tao, J.T.S. Irvine, Adv. Mater. 18 (2006) 1581.
[23] P. Babilo, S. Haile, J. Am. Ceram. Soc. 88 (2005) 2362.
[24] D.R. Lide, Handbook of Chemistry and Physics, 76th ed., CRC Press, 1995–96.
[25] M.J. Verkerk, A.J.A. Winnubst, A.J. Burggraff, J. Mater. Sci. 17 (1982) 3113.
[26] R.V. Wilhelm Jr., D.S. Howarth, Ceram. Bull. 58 (1979) 228.
[27] A.J. Feighery, J.T.S. Irvine, Solid State Ionics 121 (1999) 209.
[28] C. Kleinlogel, L.J. Gauckler, Solid State Ionics 135 (2000) 567.
[29] T. Takada, S.F. Wang, S. Yoshikawa, S.J. Jang, R.E. Newnham, J. Am. Ceram. Soc. 77 (1994) 2485.
[30] D.W. Kim, D.G. Lee, K.S. Hong, Mater. Res. Bull. 36 (2001) 585.
[31] U. Spitsbergen, Acta Crystallogr. 13 (1960) 197.
[32] R.D. Shannon, Acta Crystallogr. A 32 (1976) 751.
[33] A.C. Larson, R.B. Von Dreele, GSAS-Generalised Crystal Structure Analysis System, Los Alamos National Laboratory Report no. LA-UR-86-748, 1994.
[34] P.T. Woodward, Acta Crystallogr. B 53 (1997) 32.
[35] K.S. Knight, N. Bonanos, Solid State Ionics 77 (1996) 189.
[36] W.S. Wang, A.V. Virkar, J. Power Sources 142 (2005) 1.
[37] F.T. Ciacchi, S.A. Nightingaleb, S.P.S. Badwal, Solid State Ionics 86-88 (1996) 1167.

[38] T. Ishihara, H. Matsuda, Y. Takita, J. Am. Chem. Soc. 116 (1994) 3801.

[39] B.C.H. Steele, Mater. Sci. Eng. B Solid 13 (1992) 79.

[40] T. Schneller, T. Schober, Solid State Ionics 164 (2003) 131.

[41] B.C.H. Steele, A. Heinzel, Nature 414 (2001) 345.

[42] L.S. Cavalcante, M. Anicete-Santos, F.M. Pontes, I.A. Souza, L.P.S. Santos, I.L.V. Rosa, M.R.M.C. Santos, L.S. Santos-Junior, E.R. Leite, E. Longo, J. Alloys Compds. 437 (2007) 269.